SCIENTIFIC REPORTS

OPEN

# Direct Studies on the Lithium-Storage Mechanism of Molybdenum Disulfide

Received: 16 March 2017
Accepted: 30 June 2017
Published online: 04 August 2017

Qingmei Su[1,2], Shixin Wang[1], Miao Feng[3], Gaohui Du[1,3] & Bingshe Xu[1,4]

**Transition metal sulfides are regarded as a type of high-performance anode materials for lithium ion batteries (LIBs). However, their electrochemical process and lithium-storage mechanism are complicated and remain controversial. This work is intended to give the direct observation on the electrochemical behavior and find out the lithium-storage mechanism of molybdenum disulfide ($MoS_2$) using *in situ* transmission electron microscopy (TEM). We find that single-crystalline $MoS_2$ nanosheets convert to Mo nanograins (~2 nm) embedded in $Li_2S$ matrix after the first full lithiation. After the delithiation, the Mo nanograins and $Li_2S$ transform to a large number of lamellar $MoS_2$ nanocrystals. The discharge-charge cycling of $MoS_2$ in LIBs is found to be a fully reversible conversion between $MoS_2$ and Mo/$Li_2S$ rather than the electrochemical conversion between S and $Li_2S$ proposed by many researchers. The *in situ* real-time characterization results give direct evidence and profound insights into the lithium-storage mechanism of $MoS_2$ as anode in LIBs.**

The widespread application of lithium ion batteries (LIBs) promotes extensive studies on high-performance electrode materials[1,2]. Graphite materials are generally used as anodes in commercial LIBs owing to their low cost, low working potential, and structural stability. However, the relatively low capacity (about 372 mAh $g^{-1}$) of graphite materials cannot meet the requirement of large-scale LIBs in the future[3,4]. To solve the problem, great efforts have been made to find promising anode materials to replace graphite[5–7]. As a typical layered transition metal sulfide, $MoS_2$ has a layered structures consisting of covalently bound S-Mo-S trilayers; the $MoS_2$ layers are bonded by a relatively weak van der Waals force. These structural features make $MoS_2$ suitable for the intercalation of lithium ions[8]. $MoS_2$ is a promising anode material because its theoretical capacity (670 mAh $g^{-1}$ assuming 4 moles of $Li^+$ insertion) can be three and a half times that of commercial graphite anodes (372 mAh $g^{-1}$)[9–11]. Besides, compared to other emerging anode materials (like Ge and Si), $MoS_2$ generally demonstrates high capacity retention and excellent rate capability. Especially, nanostructured $MoS_2$-based anodes have been extensively studied and their electrochemical performances have been further improved[12–17].

Researches on the reaction mechanism of $MoS_2$ as anode in LIBs are significant for both fundamental studies and practical applications. The intercalation of lithium ions into $MoS_2$ happens in the voltage range of 3.0–0 V with varied reaction mechanisms. Lithium intercalation is believed to be reversible in the voltage of 3–1.1 V via the reaction: $MoS_2 + xLi^+ + xe^- \leftrightarrow Li_xMoS_2$. At voltages below 1.1 V there exist one or several electrochemical reactions along with the formation of intermediate metastable sulfides. The complex mechanism of lithium intercalation into $MoS_2$ under deep discharge has been preliminarily investigated. Different reaction mechanisms for the conversion process of $MoS_2$ with Li have been recently proposed by various groups. Lemmon and co-workers reported that $MoS_2$ was reduced to metallic Mo and $Li_2S$ at 0.01 V (*vs.* Li/$Li^+$)[18]. Wang and Li believed that the lithium storage mechanism of $MoS_2$ is a reversible phase transformation between $MoS_2$ and Mo/$Li_2S$[19], and major researches agree with this reversible conversion mechanism[20–25]. However, many groups suggested that the conversion mechanism of $MoS_2$ is analogous with Li–S battery due to the formation of $Li_2S$ during the first discharge process according to the redox chemistry[12,26–28]; the subsequent reaction is a reversible conversion between $Li_2S$ and elemental sulfur: $Li_2S \leftrightarrow S + 2Li$. It says metallic Mo is not active and $Li_2S$/S is the electrochemical reaction

[1]Institute of Atomic and Molecular Science, Shaanxi University of Science and Technology, Xi'an, 710021, China. [2]Zhejiang Provincial Key Laboratory of Solid State Optoelectronic Devices, Zhejiang Normal University, Jinhua, 321004, China. [3]Institute of Physical Chemistry, Zhejiang Normal University, Jinhua, 321004, China. [4]Research Centre of Advanced Materials Science and Technology, Taiyuan University of Technology, Taiyuan, 030024, China. Correspondence and requests for materials should be addressed to Q.S. (email: suqingmei@zjnu.cn) or G.D. (email: dugaohui@sust.edu.cn)

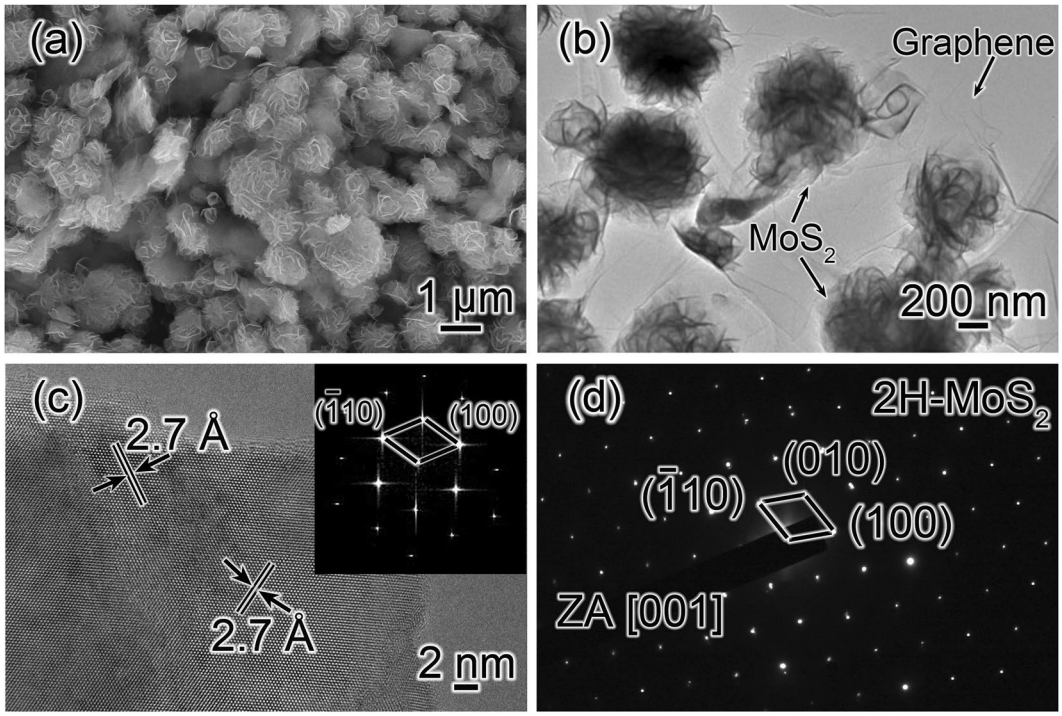


**Figure 1.** (**a**) SEM and (**b**) TEM images of the $MoS_2$/graphene products. (**c**) HRTEM image and (**d**) SAED pattern of an individual $MoS_2$ nanosheet. The inset of (**c**) is the corresponding FFT pattern of the HRTEM image.

couple in a deeply discharged $MoS_2$/Li cell. Thus, the electrochemical reaction between $MoS_2$ and Li needs thorough enlightenment owing to these controversial results.

Considerable understandings of $MoS_2$ were achieved by examining the electrode materials after charge or discharge by disassembling the conventional LIBs (i.e. *ex situ*); no report provided direct reaction behavior of $MoS_2$ electrode during the discharge-charge cycling to analyze the lithium-storage mechanism. *In situ* TEM is an advanced technique that allows specific nanoscale site on the materials to be monitored in real-time[29–37]. The lithium intercalation into $MoS_2$ nanosheet has been reported by Bai's group through *in situ* TEM approach[36], and they demonstrated a phase conversion from pristine 2H-$MoS_2$ to 1T-$LiMoS_2$. Their finding confirms the initial $Li^+$ intercalation mechanism into $MoS_2$. The controversial conversion mechanism involving the deep discharge of the battery (at approximate 0 V *vs*. $Li/Li^+$) is not resolved. Particularly, the microstructural evolution of $MoS_2$ electrode during continuous discharge-charge cycling remains unknown.

In this work, we investigated the lithium intercalation and conversion process of lamellar $MoS_2$ nanosheets in deep cycle (like the battery operation between 0–3 V) by *in situ* TEM, and realized a real-time observation of the electrochemical lithiation and delithiation process that greatly advances the understanding of the intercalation and conversion mechanism of $MoS_2$ in LIBs. The experimental results, for the first time, thoroughly demonstrate the structural transition of $MoS_2$ is reversible in the full discharge-charge cycling. Our findings shed light on the electrochemical reaction of $MoS_2$ with lithium and benefit for future material design and applications in energy conversion and storage devices.

## Results

The morphology and microstructure of the synthesized $MoS_2$/graphene were analyzed by SEM and TEM. Figure 1(a) presents a SEM image of the obtained $MoS_2$/graphene used in this study; the $MoS_2$/graphene is composed of many uniform $MoS_2$ microspheres with sizes of 1–2 μm. Figure 1(b) clearly reveals the microstructures of the $MoS_2$ microspheres anchored on graphene nanosheet. It can be seen that the hierarchical flower-like microspheres are regularly composed of numerous thin nanosheets. Figure 1(c) shows a HRTEM image of an individual $MoS_2$ sheet in the microspheres. The marked interplanar spacing of 2.7 Å corresponds to the (100) and ($\bar{1}$10) lattice planes of the hexagonal $MoS_2$ phase, respectively. The inset is the corresponding fast Fourier transform (FFT) pattern of the HRTEM image. The SAED pattern recorded from an individual $MoS_2$ nanosheet shows clear diffraction spots and can be well indexed as (100), (010) and ($\bar{1}$10) planes of pure hexagonal $MoS_2$ along the[001] zone axis (JCPDF No. 87-2416), indicating a high crystallinity of $MoS_2$ phase.

We prepared an all-solid nanoscale LIB inside the TEM that enabled the *in situ* electrochemical experiments of $MoS_2$/graphene. Graphene nanosheets in the composite were used as substrate to support the $MoS_2$ nanostructures so that the *in situ* observation could be easily performed. The nanosized electrochemical cell consisted of three parts: $MoS_2$/graphene working electrode, Li metal counter electrode, and naturally grown $Li_2O$ on Li metal surface used as solid electrolyte. The TEM images of $Li/Li_2O$ electrode are shown in Fig. S1 in Supporting

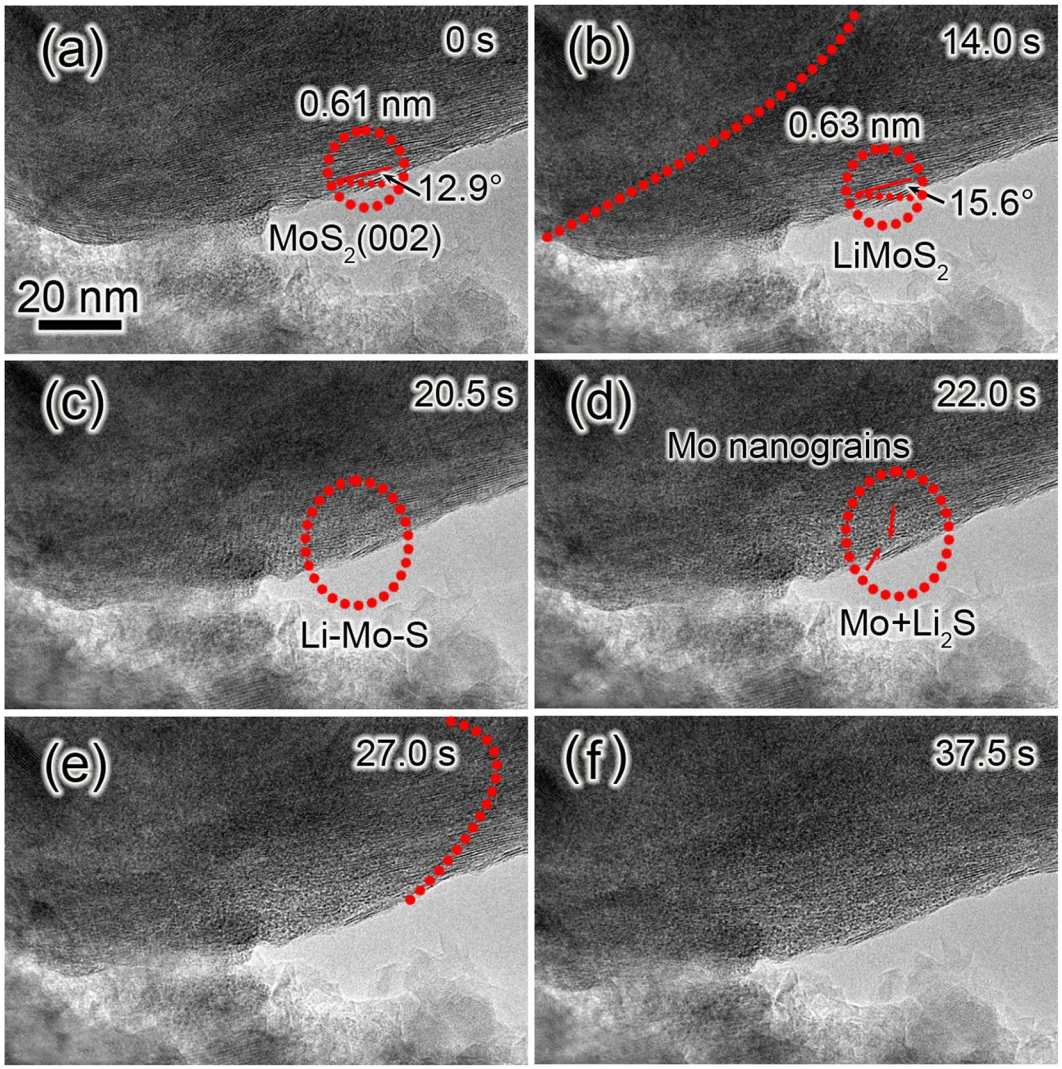


**Figure 2.** *In situ* TEM study on the lithiation of an individual $MoS_2$ nanosheet. (**a**–**f**) Time-resolved TEM images of the first lithiation process. All the scale bars are 10 nm.

Information. ED pattern and elemental mapping analysis confirm the existence of $Li_2O$ layer on Li metal. So the $MoS_2$/graphene electrode is not directly contacted with lithium metals; the observed reaction is an electrochemical process rather than electrical short-circuit. Subsequently, the electrochemical conversion reaction of $MoS_2$ nanosheets during the first lithiation process was investigated. Figure 2 shows a series of time-resolved TEM images of a $MoS_2$ nanosheet during the first lithiation, which is a screenshot from Movie S1 in Supporting Information. The marked interplanar spacing of 0.61 nm corresponds to the (002) lattice plane of the hexagonal $MoS_2$ phase. Figure 2(a) was used as the starting point to monitor the progress of the lithiation reaction. Three stages in the first lithiation process can be discerned from Movie S1 in the Supporting Information. The first stage, from 0 to 14.0 s, indicates the initial $Li^+$ intercalating reaction with $MoS_2$. We can see the slight variation of the orientation of lattice fringes in the TEM images and Movie S1 due to the strain induced by the lithium intercalation, leading to the formation of $Li_xMoS_2$ phase via 2H-1T transformation[36]. The lattice fringes of 0.63 nm in Fig. 2(b) corresponds to the (001) lattice plane of the $LiMoS_2$ phase (JCPDF No. 44-1078). The images recorded from 14.0 s to 27 s are the second stage (Fig. 2b–e), in which the crystalline $MoS_2$ layers began to collapse, leading to the formation of small Mo-Li-S clusters and then Mo clusters and $Li_2S$ phase. In Fig. 2(c–e), many nanodots resulted from the decomposition of a $MoS_2$ monolayer should be Mo clusters. In the stage three, Mo clusters aggregated and grew into Mo nanograins as shown in Fig. 2(f). The continuous lithiation was revealed by the change of the texture of $MoS_2$ nanosheet in the TEM images. Most of the lattice fringes of $MoS_2$ nanosheet disappeared and numerous ultrafine nanograins were formed owing to lithiation reaction in Fig. 2(f).

Figure 3(a) is a TEM image of a pristine $MoS_2$ microsphere; the initial size of the marked $MoS_2$ nanosheet was 133 nm. After the first full lithiation, the size of $MoS_2$ nanosheet increased to 145 nm as shown in Fig. 3(b), and the corresponding size expansion was ~8.8%. The TEM images of an individual $MoS_2$ nanoflake after the first lithiation are shown in Fig. 3(c,d). The surface and edges of the lithiated $MoS_2$ nanoflake were coated by a uniform layer of crystallite with a thickness of 8–9 nm, which was identified to be $Li_2S$ from the ED pattern in Fig. 3(f).

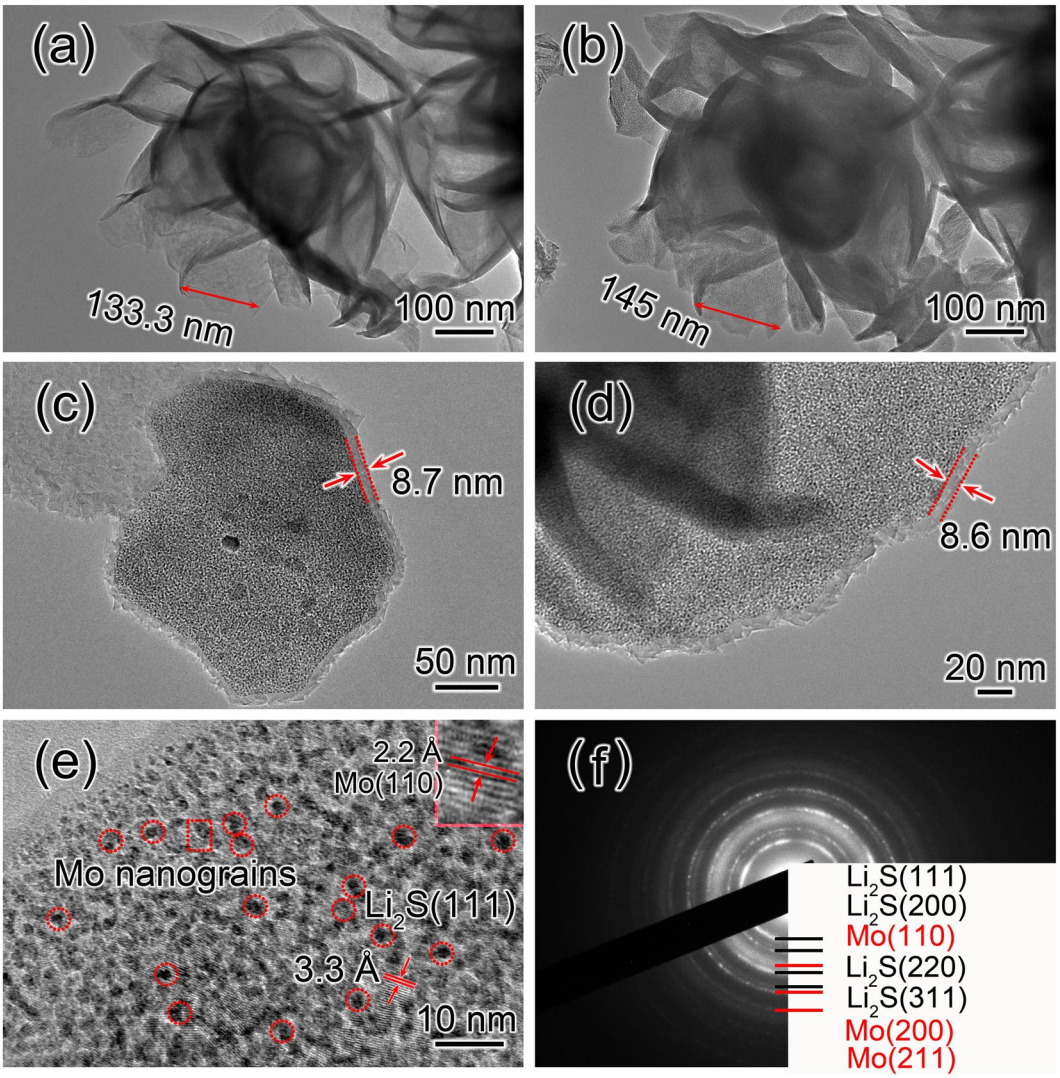


**Figure 3.** (**a**) TEM image of a pristine $MoS_2$ microsphere before lithiation. (**b**) TEM image of $MoS_2$ microsphere after first lithiation. (**c**,**d**) TEM images of the lithiated $MoS_2$ nanoflakes selected from the $MoS_2$ electrode in (**b**). (**e**) HRTEM image and (**f**) ED pattern of the fully lithiated $MoS_2$ microsphere in (**b**).

Figure 3(e) shows the detailed structure information of the lithiated $MoS_2$ nanoflake, which is composed of numerous nanograins around 2 nm. The HRTEM image of a nanograin in the lithiated $MoS_2$ nanoflake gives the lattice fringes of 2.2 Å (the inset of Fig. 3e), which is agreed with the lattice spacing of (110) plane of Mo (JCPDF No. 89-5156). The fringe spacing of the matrix was measured to be 3.3 Å, corresponding to the (111) plane of $Li_2S$ (77–2145). The dense Mo nanograins form an interconnected network that works as an efficient conductive pathway for electron transport into the $MoS_2$, while the $Li_2S$ provides a similar pathway for Li ions during electrochemical reaction. Since $Li_2S$ has a much smaller density (1.66 g/cm$^3$) than that of metal Mo (10.28 g/cm$^3$), the volumetric expansion of $MoS_2$ electrode during the lithiation process is mainly caused by the formation of $Li_2S$ with lower density. $Li_2S$ is soft and the resulted $Li_2S$ in the nanoflakes could be partially squeezed out of the Mo network/framework due to volumetric expansion. So $Li_2S$ shells with a thickness of 8–10 nm were formed around the fully lithiated nanoflakes. Figure 3(f) is the ED pattern of the fully lithiated $MoS_2$ electrode. All the diffraction rings are well indexed into Mo and $Li_2S$. The results demonstrate the lithiation reaction involves the reduction of $MoS_2$ to Mo nanograins accompanying with the formation of $Li_2S$. The whole lithiation reaction can be expressed as the following equation: $MoS_2 + 4Li^+ + 4e^- \rightarrow Mo + 2Li_2S$.

After the first lithiation process, a potential of +3.0 V was applied to the lithiated $MoS_2$ electrode to initiate the delithiation reaction. The time-resolved TEM images of the electrode during the delithiation are shown in Fig. 4. Figure 4(a) is a TEM image of the lithiated $MoS_2$ electrode, in which numerous Mo nanograins (black nanodots) around 2 nm are embedded in the $Li_2S$ matrix. After the delithiation reaction for 383 s (Fig. 4b), an obvious change could be observed in the nanosheet electrode in comparison to the image in Fig. 4a. The Mo nanograins became smaller due to the electrochemical reaction with $Li_2S$ during delithiation. As the delithiation reaction proceeded, black nanodots involving Mo nanograins almost disappeared, and the electrode turned to

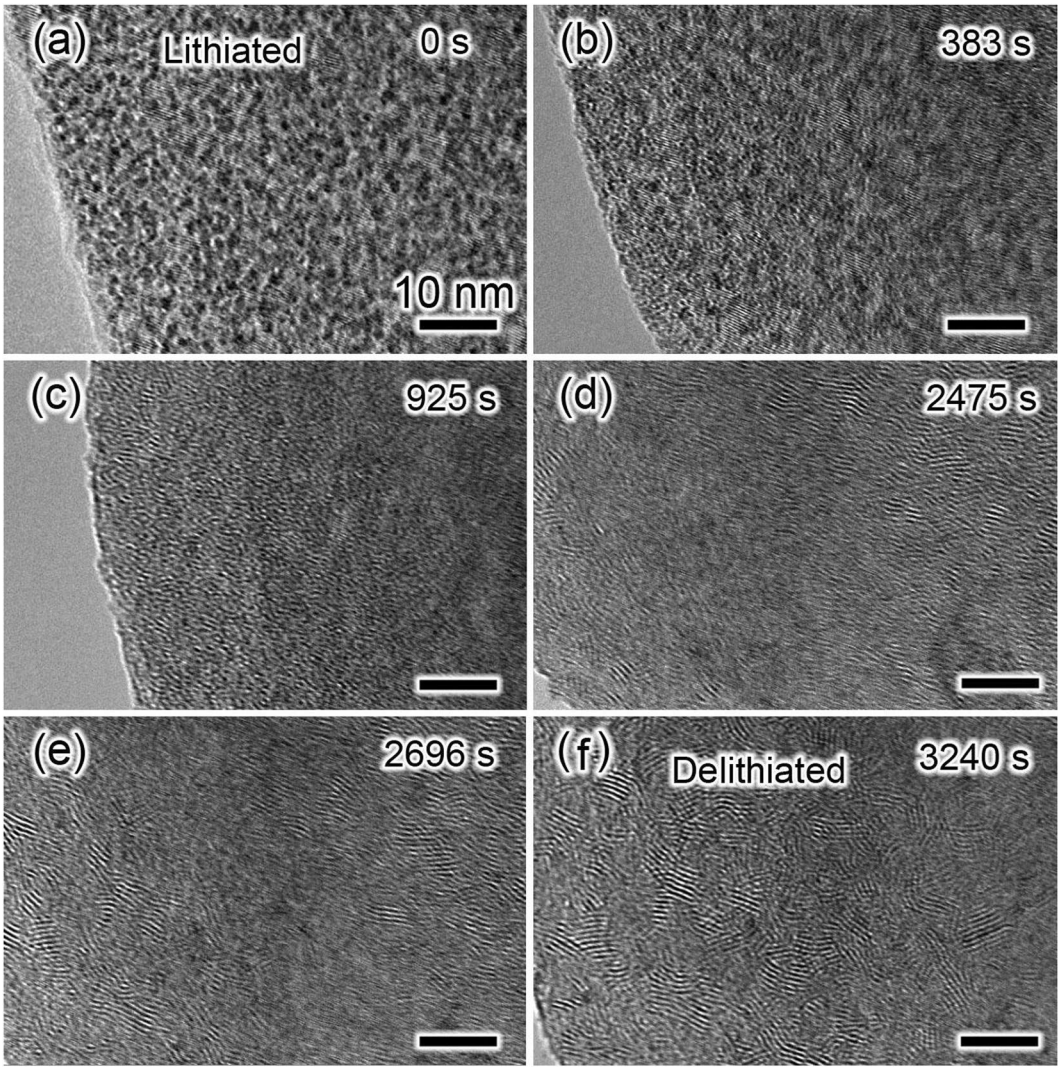


**Figure 4.** Time-resolved TEM images of a lithiated $MoS_2$ nanosheet during the delithiation process showing obvious microstructure and phase evolution as a function of time. (**a**) 0 s, (**b**) 383 s, (**c**) 925 s, (**d**) 2475 s, (**e**) 2696 s and (**f**) 3240 s. All the scale bars are 10 nm.

an approximately amorphous texture after 925 s (Fig. 4c). Obvious formation of lattice fringes in the electrode was observed at 2475 s during the delithiation process (Fig. 4d). After reaction for 3240 s (Fig. 4f), we found the perfect lattice fringes were formed, indicating the completion of delithiation reaction.

The delithiated $MoS_2$ electrode was analyzed using TEM. Figure 5(a) is a TEM image of the delithiated $MoS_2$ electrode. It can be clearly seen that the thin $Li_2S$ shell on lithiated nanosheets was disappeared. The magnified TEM image of the delithiated $MoS_2$ nanosheet is displayed in Fig. 5(b), suggesting that a large number of lamellar nanocrystals with a size of 3–5 nm formed during the delithiation process, as marked by the red circles. Figure 5(c) is a HRTEM image of the delithiated $MoS_2$ nanosheet; the interplanar distance of nanograins was measured to be 6.1 Å, which can be indexed as the (002) lattice planes of the hexagonal $MoS_2$ phase (JCPDF No. 87-2416). The ED pattern of the delithiated nanosheet is shown in Fig. 5(d); all the diffraction rings can be indexed as the hexagonal $MoS_2$ phase (JCPDF No. 87-2416). The HRTEM and ED results reveal that metallic Mo nanograins convert to $MoS_2$ nanograins in the delithiation process. Here molybdenum oxide was not observed during the delithiation process although $Li_2O$ electrolyte was contacted with the electrode. The electrochemical reaction in the delithiation process can be expressed as $Mo + 2Li_2S \rightarrow MoS_2 + 4Li^+ + 4e^-$.

$MoS_2$ materials showed excellent cyclability during the charge-discharge cycles in LIBs[12–14]. *In situ* TEM experiments were performed to reveal the microstructure and phase evolution induced by the continual lithiation-delithiation in the discharge-charge cycles. Figure 6(a) is a TEM image of the pristine $MoS_2$ electrode, and the insets is a HRTEM image of the $MoS_2$ nanosheet. The marked interplanar spacing of 2.7 Å corresponds to the (100) and ($\bar{1}$10) lattice planes of the hexagonal $MoS_2$ phase, respectively. The ED pattern of the pristine $MoS_2$ nanosheet is displayed in Fig. 6($a_1$). It can be indexed as (100), (010) and ($\bar{1}$10) planes of pure hexagonal $MoS_2$ phase along the[001] zone axis (JCPDF No. 87-2416). Figure 6(b) is a TEM image of $MoS_2$ nanosheet after the first lithiation, and a thin $Li_2S$ shell with a thickness of 8–9 nm was formed on the lithiated nanosheet. Meanwhile

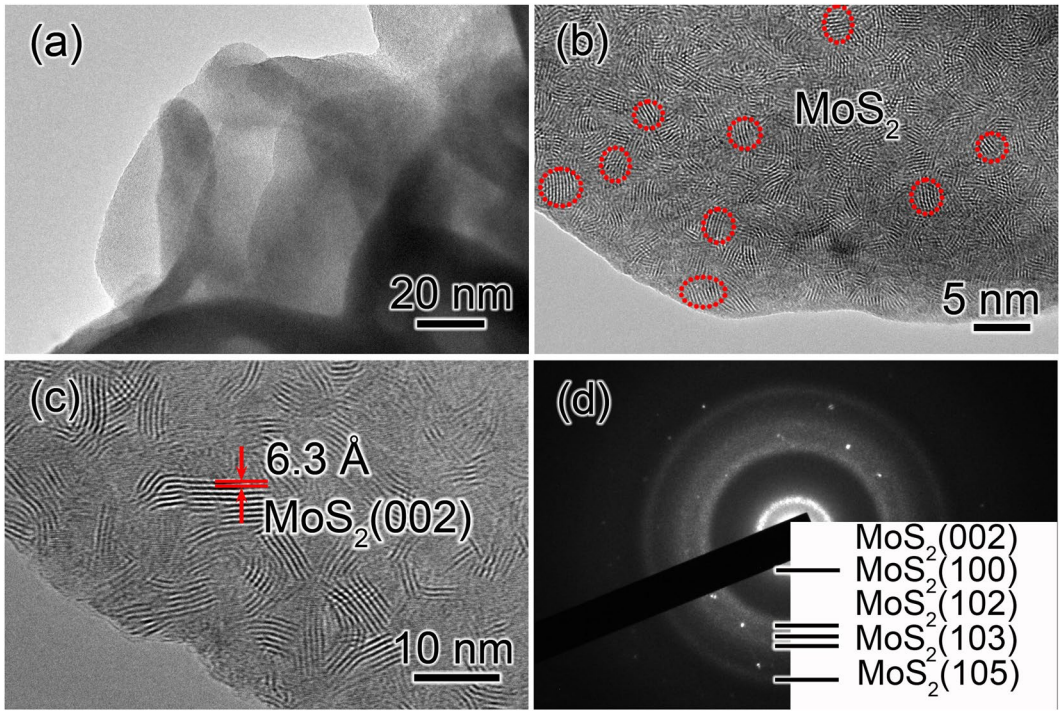


**Figure 5.** (**a**) TEM image of $MoS_2$ electrode after delithiation with a potential of +3.0 V. (**b**) The enlarged TEM image of a delithiated $MoS_2$ sheet. (**c**) HRTEM image and (**d**) ED pattern of a delithiated $MoS_2$ nanosheet.

numerous Mo nanograins (~2 nm) were formed and embedded in $Li_2S$ matrix during the lithiation reaction. The corresponding ED pattern of the lithiated $MoS_2$ electrode is shown in Fig. 6($b_1$). The diffraction rings can be well indexed to Mo and $Li_2S$, suggesting the conversion of $MoS_2$ to Mo and $Li_2S$ in the first lithiation process. The potential was reversed to +3 V to initiate the delithiation process after the completed lithiation. Figure 6(c) is the TEM image of the delithiated $MoS_2$ electrode. It shows that the thin $Li_2S$ shell disappeared. The Mo nanograins transformed into a large number of $MoS_2$ nanograins with sizes of 3–5 nm during the delithiation reaction, as marked by the red circles. Figure 6($c_1$) displays the ED pattern of the delithiated $MoS_2$ electrode; the diffraction rings all originate from lattice planes of the hexagonal $MoS_2$ phase (JCPDF No. 87-2416). The second lithiation process proceeded with the potential of −1.0 V again as shown in Fig. 6(d). Movie S2 in the Supporting Information also reveals the dynamic conversion of the electrode material in the second lithiation process. The $Li_2S$ layer formed and continued to cover the electrode like the first lithiation. The ED pattern of the secondly lithiated electrode is shown in Fig. 6($d_1$) and can be indexed as Mo and $Li_2S$. The $Li_2S$ layer and Mo nanograins disappeared again in the second delithiation process (Fig. 6e), showing a reversible phase change. The ED pattern in Fig. 6($e_1$) indicated the resultant Mo/$Li_2S$ converted to $MoS_2$ nanograins again in the second delithiation process. The two cycles indicate that a reversible electrochemical conversion between $MoS_2$ and Mo/$Li_2S$ takes place in the whole cycling, and the electrochemical reaction in the discharge-charge cycling can be expressed as $MoS_2 + 4Li^+ + 4e^- \leftrightarrow Mo + 2Li_2S$.

The electrochemical performances of $MoS_2$/graphene electrode in coin cells were tested. As shown in Fig. S2, the initial discharge and charge capacities are 2018 mAh $g^{-1}$ and 1609 mAh $g^{-1}$, respectively. After 100 cycles, the reversible capacity of the $MoS_2$/graphene electrode remains 1002 mAh $g^{-1}$, demonstrating a high lithium–storage capability and excellent cycling performance. The reversible capacity is higher than the theoretic capacity of $MoS_2$, which can be attributed to the synergistic effects of graphene and the reversible formation/decomposition of SEI membrane.

The *in situ* TEM results were further supported by *ex situ* TEM results, as displayed in Fig. S3 in Supporting Information. The TEM image of the $MoS_2$/graphene electrode after 50 discharge-charge cycles shows that numerous ultrafine nanograins were formed (Fig. S3(a)). The stripe-width of the crystallites is 2.2 Å, which corresponds to the interplanar spacing of Mo (110) plane (Fig. S3(b)). The HRTEM analysis confirms the formation of Mo nanograins after discharge. Meanwhile, Fig. R3(c) and (d) indicate that the $MoS_2$ phase was obtained after charge. The *ex situ* TEM results are well agreed with our *in situ* TEM results, and confirms the same conversion mechanism revealed by *in situ* TEM. The findings clarified the lithium-storage mechanism of $MoS_2$ involving the reversible phase transformation between Mo nanograins and $MoS_2$ nanograins along with the reversible growth/decomposition of $Li_2S$ during cycling. The reactions are analogous to the electrochemical conversion of $CoS_2$[38], and most transition-metal oxides[39]. Thus, the electrochemically active couple in $MoS_2$ electrode is not S/$Li_2S$ but $MoS_2$ and Mo/$Li_2S$ in a deeply discharged/charged $MoS_2$/Li system.

Our *in situ* and *ex situ* TEM results reveal a reversible phase conversion during the lithitation-delithiaton processes of $MoS_2$. However, the typical CV curves of $MoS_2$ in literatures generally show distinct 1st and

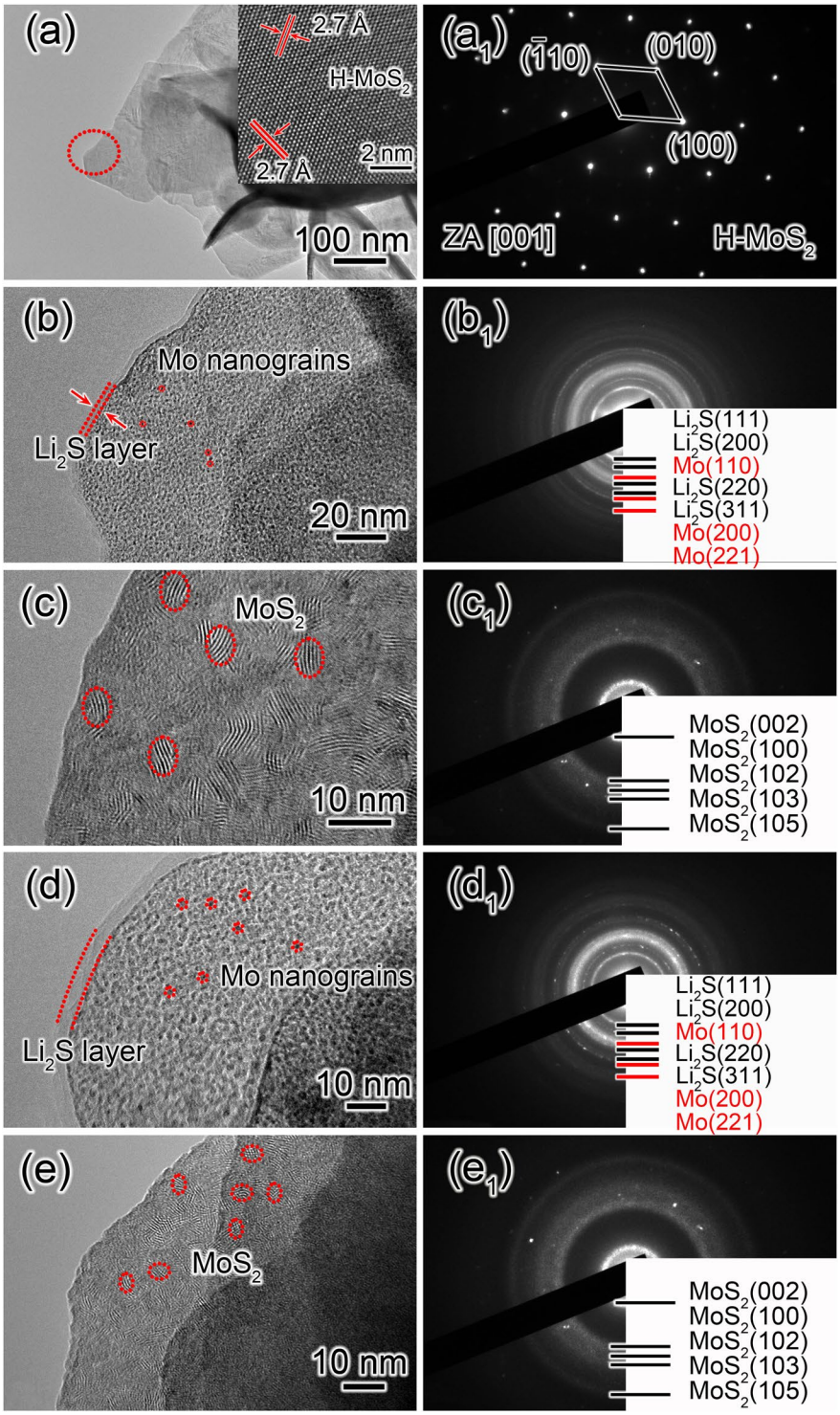


**Figure 6.** Morphology and structure evolution of $MoS_2$ electrode during cycling with the potential of −1.0 V for lithiation and +3.0 V for delithiation. (**a**) TEM image of the pristine $MoS_2$ nanosheet. (**b**,**c**) TEM images of $MoS_2$ nanosheet after the first lithiation and delithiation. (**d**,**e**) TEM images of $MoS_2$ nanosheet after the second lithiation and delithiation. ($\mathbf{a_1}$–$\mathbf{e_1}$) The corresponding ED patterns of the $MoS_2$ electrode in (**a**–**e**).

subsequent discharge processes[40–43]. The difference in the CV curves may be caused by the irreversible processes such as the decomposition of electrolyte in the first discharge[40], the formation of a solid-electrolyte interface (SEI) layer resulting from the continual reaction of freshly exposed surfaces of electrode materials with the organic electrolyte[41], and particularly the structural rearrangement revealed by our TEM observation in the first discharge-charge process from micro-sized $MoS_2$ nanosheets to numerous $MoS_2$ nanograins of 3–5 nm, which possess distinct quantum and size effects. Besides, the $MoS_2$ nanostructures prepared by the hydrothermal or

solution method contain many defect sites. A fraction of lithium ions can be trapped in the defect sites and hardly extracted in the following cycles[42]. The residual oxygen-containing groups in graphene for $MoS_2$/graphene composite are also electrochemical reduced in the first discharge[43]. All these irreversible processes can cause different reaction thermodynamics between the 1st and subsequent discharge. The underlying mechanism still needs thorough investigation.

## Conclusions

In summary, we have conducted a systematical study of the structural evolution of $MoS_2$ nanosheets during the lithiation-delithiation cycling using *in situ* TEM technique by constructing a nano-LIB device inside a TEM. In our experiments, the details of Li-ion intercalation and extraction-induced solid-state phase transformation in $MoS_2$ are clearly understood. The results demonstrate that single-crystalline $MoS_2$ nanosheets transform to multicrystalline nanosheets consisting of many Mo nanograins embedded in $Li_2S$ matrix during the first lithiation. Generally, a uniform layer of $Li_2S$ with thickness of 8–9 nm can be observed on the lithiated electrode. During the delithiation process, Mo nanograins and $Li_2S$ layer convert to a large number of lamellar $MoS_2$ nanograins with sizes of 3–5 nm. The charge-discharge processes of $MoS_2$ in LIBs are not the controversial electrochemical conversion between S and $Li_2S$ but a fully reversible phase conversion between $MoS_2$ nanograins and Mo nanograins along with the formation/decomposition of $Li_2S$. Based on our *in situ* TEM results, the electrochemical conversion mechanism of $MoS_2$ in LIBs is: $MoS_2 + 4Li^+ + 4e^- \leftrightarrow Mo + 2Li_2S$. The *in situ* real-time characterization results provide direct evidence and achieve a profound understanding of the lithium-storage mechanism in $MoS_2$.

## Methods

**Materials synthesis.** Graphene Oxide (GO) was prepared by oxidization of natural graphite flakes using a modified Hummers method[44]. For the synthesis of $MoS_2$/graphene, GO (0.06 g) was added into 20 mL of deionized water with sonication for 1 h to form a homogeneous dispersion. Then 0.3 g of $Na_2MoO_4{\cdot}2H_2O$, 0.4 g of thiourea, and 0.15 g of PEG-20000 were added. After ultrasonication and stirring for 30 min, the solution was then transferred into a Teflon-lined stainless steel autoclave, sealed tightly, and heated at 200 °C for 24 h. The black products were collected by centrifugation, washed with deionized water and ethanol, and dried in a vacuum oven at 60 °C for 24 h. The obtained composites were annealed in a tube furnace at 800 °C for 2 h in a stream of hydrogen (20 sccm) and argon (180 sccm).

***In situ* electrochemical experiments inside TEM.** The *in situ* nanoscale electrochemical experiments were performed using a Nanofactory STM-TEM holder inside a TEM (JEOL JEM-2100F). $MoS_2$/graphene samples were attached to a gold wire and served as the working electrode; a lithium particle on the tip of a W rod was served as the counter electrode and lithium source. Both the $MoS_2$/graphene and lithium electrodes were loaded onto a Nanofactory STM-TEM holder inside a glovebox and sealed in an argon-filled bag. Then the holder was transferred into the TEM column quickly. A thin $Li_2O$ layer was formed on the surface of the metallic lithium particle due to the exposure to air during the transfer process and was served as the solid electrolyte. Once the $Li_2O$-covered Li electrode driven by the mobile STM probe contacted the free end of the selected lamellar $MoS_2$/graphene, a negative bias (−1.0 V) was applied to drive $Li^+$ transport through the solid-state $Li_2O$ layer to facilitate the lithiation. The current of about tens or hundreds nA passed through the sample during the reaction (dependent on the size of the selected sample). Then a bias was reversed to be positive (+3.0 V) to initiate the delithiation process. To minimize the electron beam irradiation effect on the microstructure and the electrochemical behavior, the experiments were carried out with the electron beam blanked except for imaging. During the image acquisition, the total dose of electron beam was reduced with sacrifice in resolution and contrast. In some cases, the beam radiation was performed in a sacrificial region and the TEM measurements were taken on a nearby region that had not been previously exposed to the electron beam.

## References


1. Armand, M. & Tarascon, J. M. Building better batteries. *Nature* **451**, 652–657 (2008).
2. Kim, W. S., Choi, J. Y. & Hong, S. H. Meso-porous silicon-coated carbon nanotube as an anode for lithium-ion battery. *Nano Res.* **9**, 2174–2181 (2016).
3. Cao, F. F. *et al*. Cu-Si nanocable arrays as high-rate anode materials for lithium-ion batteries. *Adv. Mater.* **23**, 4415–4420 (2011).
4. Liang, Y. L. *et al*. Rechargeable Mg batteries with graphene-like $MoS_2$ cathode and ultra small Mg nanoparticle anode. *Adv. Mater.* **23**, 640–643 (2011).
5. Liu, Y. C., Zhao, Y. P., Jiao, L. F. & Chen, J. A. Graphene-like $MoS_2$/graphene nanocomposite as a high performance anode for lithium ion batteries. *J. Mater. Chem. A* **2**, 13109–13115 (2014).
6. Yao, Y. *et al*. Interconnected silicon hollow nanospheres for lithium-ion battery anodes with long cycle life. *Nano. Lett.* **11**, 2949–2954 (2011).
7. Cho, J. S., Hong, Y. J. & Kang, Y. C. Design and synthesis of bubble-nanorod-structured $Fe_2O_3$-carbon nanofibers as advanced anode material for Li-ion batteries. *ACS Nano* **9**, 4026–4035 (2015).
8. Stephenson, T., Li, Z., Olsen, B. & Mitlin, D. Lithium ion battery applications of molybdenum disulfide ($MoS_2$) nanocomposites. *Energy Environ. Sci.* **7**, 209–231 (2014).
9. Xie, Y. & Wu, C. Z. Design of nanoarchitectured electrode materials applied in new-generation rechargeable lithium ion batteries. *Dalton Trans.* **45**, 5235–5240 (2007).
10. Li, H., Li, W. J., Ma, L., Chen, W. X. & Wang, J. M. Electrochemical lithiation/delithiation performances of 3D flowerlike $MoS_2$ powders prepared by ionic liquid assisted hydrothermal route. *J. Alloys Compd.* **471**, 442–447 (2009).
11. Wang, Y., Li, H., He, Hosono, P. & Zhou, E. H. Nano active materials for lithium-ion batteries. *Nanoscale* **2**, 1294–1305 (2010).
12. Zhou, J. W. *et al*. 2D space-confined synthesis of few-layer $MoS_2$ anchored on carbon nanosheet for lithium-ion battery anode. *ACS Nano* **9**, 3837–3848 (2015).
13. Li, H. S. *et al*. Enhanced lithium-storage performance from three-dimensional $MoS_2$ nanosheets/carbon nanotube paper. *Chem. Electro. Chem.* **1**, 1118–1125 (2014).

14. Zhang, K. *et al*. Graphene/acid coassisted synthesis of ultrathin $MoS_2$ nanosheets with outstanding rate capability for a lithium battery anode. *Inorg. Chem.* **52**, 9807–9812 (2013).
15. Hu, L. R., Ren, Y. M., Yang, H. X. & Xu, Q. Fabrication of 3D hierarchical $MoS_2$/polyaniline and $MoS_2$/C architectures for lithium-ion battery applications. *ACS Appl. Mater. Interfaces* **6**, 14644–14652 (2014).
16. Rao, C. N. R., Gopalakrishnan, K. & Maitra, U. Comparative study of potential applications of graphene, $MoS_2$, and other two-dimensional materials in energy devices, sensors, and related areas. *ACS Appl. Mater. Interfaces* **7**, 7809–7832 (2015).
17. Gao, M. R., Xu, Y. F., Jiang, J. & Yu, S. H. Nanostructured metal chalcogenides: synthesis, modification, and applications in energy conversion and storage devices. *Chem. Soc. Rev.* **42**, 2986–3017 (2013).
18. Xiao, J. *et al*. Exfoliated $MoS_2$ nanocomposite as an anode material for lithium ion batteries. *Chem. Mater.* **22**, 4522–4524 (2010).
19. Wang, Q. & Li, J. H. Facilitated lithium storage in $MoS_2$ overlayers supported on coaxial carbon nanotubes. *J. Phys. Chem. C* **111**, 1675–1682 (2007).
20. Hwang, H., Kim, H. & Cho, J. $MoS_2$nanoplates consisting of disordered graphene-like layers for high rate lithium battery anode materials. *Nano. Lett.* **11**, 4826–48360 (2011).
21. Chang, K. & Chen, W. X. *In situ* synthesis of $MoS_2$/graphene nanosheet composites with extraordinarily high electrochemical performance for lithium ion batteries. *Chem. Commun.* **47**, 4252–4254 (2011).
22. Yao, J. Y. *et al*. 3D nanostructured molybdenum diselenide/graphene foam as anodes for long-cycle life lithium-ion batteries. *Electrochimica. Acta* **176**, 103–111 (2015).
23. Yang, M. H., Ko, S., Im, J. S. & Choi, B. G. Free-standing molybdenum disulfide/graphene composite paper as a binder-and carbon-free anode for lithium-ion batteries. *J. Power Sources* **288**, 76–81 (2015).
24. Wang, Z. *et al*. CTAB-assisted synthesis of single-layer $MoS_2$-graphene composites as anode materials for Li-ion batteries. *J. Mater. Chem. A* **1**, 2202–2210 (2013).
25. Zhou, X. S., Wan, L. J. & Guo, Y. G. Synthesis of $MoS_2$nanosheet-graphene nanosheet hybrid materials for stable lithium storage. *Chem. Commun.* **49**, 1838–1840 (2013).
26. Fang, X. P. *et al*. Lithium storage in commercial $MoS_2$ in different potential ranges. *Electrochim. Acta* **81**, 155–160 (2012).
27. Pham, V. H. *et al*. Liquid phase co-exfoliated $MoS_2$-graphene composites as anode materials for lithium ion batteries. *J. Power Sources* **244**, 280–286 (2013).
28. Yamin, H. & Peled, E. Electrochemistry of a non-aqueous lithium sulfur cell. *J. Power Sources* **9**, 281–287 (1983).
29. Su, Q. M. *et al*. *In situ* transmission electron microscopy investigation of the electrochemical lithiation-delithiation of the individual $Co_9S_8$/Co-filled carbon nanotubes. *ACS Nano* **7**, 11379–11387 (2013).
30. McDowell, M. T. *et al*. *In situ* TEM of two-phase lithiation of amorphous silicon nanospheres. *Nano Lett.* **13**, 758–764 (2013).
31. Wang, C. M. *et al*. *In situ* transmission electron microscopy observation of microstructure and phase evolution in a $SnO_2$ nanowire during lithium intercalation. *Nano Lett.* **11**, 1874–1880 (2011).
32. He, Y. *et al*. *In situ* transmission electron microscopy probing of native oxide and artificial layers on silicon nanoparticles for lithium ion batteries. *ACS Nano* **8**, 11816–11823 (2014).
33. Huang, J. Y. *et al*. *In situ* observation of the electrochemical lithiation of a single $SnO_2$ nanowire electrode. *Science* **330**, 1515–1520 (2010).
34. Luo, L. L., Wu, J. S., Xu, J. M. & Dravid, V. P. Atomic resolution study of reversible conversion reaction in metal oxide electrodes for lithium-ion battery. *ACS Nano* **8**, 11560–11566 (2014).
35. Xiao, D. D. & Gu, L. Atomic-scale structure of nearly-equilibrated electrode materials under lithiation/delithiation for lithium-ion batteries. *Scientia Sinica Chimica* **44**, 295–308 (2014).
36. Wang, L. F., Xu, Z., Wang, W. L. & Bai, X. D. Atomic mechanism of dynamic electrochemical lithiation processes of $MoS_2$ nanosheet. *J. Am. Chem. Soc.* **136**, 6693–6697 (2014).
37. Su, Q. M. *et al*. Study on the electrochemical reaction mechanism of $ZnFe_2O_4$ by *in situ* transmission electron microscopy. *Scientific Reports* **6**, 28179 (2016).
38. Su, Q. M. *et al*. *In situ* transmission electron microscopy observation of electrochemical behavior of $CoS_2$ in lithium-ion battery. *ACS Appl. Mater. Interfaces* **6**, 3016–3022 (2014).
39. Su, Q. M., Xie, D., Zhang, J., Du, G. H. & Xu, B. S. *In situ* transmission electron microscopy observation of the conversion mechanism of $Fe_2O_3$/graphene anode during lithiation-delithiation processes. *ACS Nano* **7**, 9115–9121 (2013).
40. Park, S. *et al*. A facial and green strategy for the synthesis of $MoS_2$ nanospheres with excellent Li-ion storage properties. *Cryst. Eng. Comm.* **14**, 8323–8325 (2012).
41. Qin, W. *et al*. $MoS_2$-reduced graphene oxide composite via microwave assisted synthesis for sodium ion battery anode with improved capacity and cycling performance. *Electrochemica. Acta* **153**, 55–61 (2015).
42. Chang, K. & Chen, W. X. Single-layer $MoS_2$/graphene dispersed in amorphous carbon: towards high electrochemical performances in rechargeable lithium ion batteries. *J. Mater. Chem. A* **21**, 17175–17184 (2011).
43. Wang, Z. *et al*. CTAB-assisted synthesis of single-layer $MoS_2$-graphene composites as anode materials of Li-ion batteries. *J. Mater. Chem. A* **1**, 2202–2210 (2012).
44. Zhou, X. Y. *et al*. Microwave irradiation synthesis of $Co_3O_4$ quantum dots/graphene composite as anode materials for Li-ion battery. *Electrochim. Acta* **143**, 175–179 (2014).


## Acknowledgements

This work was supported by the National Natural Science Foundation of China (Nos.11574273, 11504330) and the Natural Science Foundation of Zhejiang Province (Nos. LQ15B010001, LY16B030003).

## Author Contributions

Q.S. and G.D. designed the experiments. Q.S., M.F. and S.W. fabricated the $ZnFe_2O_4$/graphene samples, carried out the *in situ* TEM experiments, analyzed data and wrote this manuscript. G.D. and B.X. revised the manuscript. All the authors contributed to the discussions and comments on the manuscript.

## Additional Information

**Supplementary information** accompanies this paper at doi:10.1038/s41598-017-07648-0

**Competing Interests:** The authors declare that they have no competing interests.

**Publisher's note:** Springer Nature remains neutral with regard to jurisdictional claims in published maps and institutional affiliations.